Solar selective performance of metal nitride/oxynitride based magnetron sputtered thin film coatings: A comprehensive review

Khalil Ibrahim[1,2], Hatem Taha[1,3], M Mahbubur Rahman[1,4], Humayun Kabir[4,5], Zhong-Tao Jiang[1]

[1]Surface Analysis and Materials Engineering Research Group
School of Engineering & Information Technology, Murdoch University, Perth, Western Australia 6150, Australia

[2]Department of Mechanical Engineering, Karbala Institute of Technology, Karbala 51214, Iraq

[3]Department of Physics, College of Education for Pure Science, Ibn Al-Haitham, University of Baghdad, Baghdad 10071, Iraq

[4]Department of Physics, Jahangirnagar University, Savar, Dhaka 1342, Bangladesh

[5]School of Metallurgy and Materials, University of Birmingham, Birmingham, United Kingdom

Corresponding author: m.rahman@murdoch.edu.au/ m.rahman@juniv.edu

Abstract

Since solar thermal collectors are considered to be the most direct way of converting the solar energy into the usable form, in the last few years growing attention has been paid to the development of transition metal nitride and metal oxynitride based thin film selective surfaces for solar-thermal collectors in order to harvest more solar energy. A solar-thermal energy system, generally, shows very high solar absorption of incident solar radiation from the solar-thermal collectors in the visible range (0.3 to 2.5 μm) and extremely low thermal losses through emission (or high reflection) in the infrared region (≥ 2.5 μm). The efficiency of a solar–thermal energy conversion system can be improved by the use of solar selective surfaces consisting of novel metallic nanoparticles surrounded in metal nitride/oxynitrides systems. In order to enhance the effectiveness of solar thermal devices, solar selective surfaces with high thermal stability are a prerequisite. Over the years, substantial efforts have been made in the field of solar selective surfaces to attain higher solar absorptance and lower thermal emittance at high temperature (above 400°C) applications. In this article, we review the present state-of-the-art transition metal nitride and/or oxynitrides based vacuum sputtered

nanostructured thin film coatings with respect to their optical and solar selective surface applications. We have also summarized the solar selectivity data from recent published literature investigations, including–discussion on some potential applications for these materials.

Keywords: Thermal collectors; solar selectivity; selective surface; solar absorptance; thermal emittance.

1. Introduction

Over the years, scientists and technologists around the world have been showing enormous research interest in investigating the transition metal nitride thin films based large band-gap semiconductors in their pure state and with various dopants, because of their widespread applications in spintronics and nonvolatile storage devices [1-3]. Binary nitride films such as AlN, GaN and InN have been extensively used in light emitters and detectors (in ultraviolet and visible range), and optical storage devices [4]. Each of these materials has a wide band-gap. Due to their exceptional thermal and chemical stability and higher physical hardness, GaN and AlN are also very popular in microelectronic applications [5]. Silicon and silicon-titanium based nitride thin films are largely used in many optical devices such as active and passive optical planar waveguides, and antireflecting coatings [6, 7]. Due to their enhanced mechanical and functional features such as superelasticity and shape memory effects, TiNi-based nitride alloys are widely used in the design of instruments, aerospace technologies and medicine [8, 9]. The incorporation of an appropriate amount of additive can remarkably improve the properties of such materials by inducing various defects such as vacancy, atom substitution, deformation, and cluster formation [10]. In a recent report, C-doping on CrAlN carried out by Zeng *et al*. [10] confirmed that C-doped dispersed clusters results in superior resistivity at low frequency. Structural, optical and electrical properties of Mn- and Cr-added GaN diluted magnetic semiconductors (DMSs) were inspected for their potential applications in electronic and spin-dependent photonics [11-13]. Endrino *et al*. [14] studied the effect of Si on the TiN and AlCrN thin films *via* XRD and NEXAFS methods. The addition of Si to the transition metal nitride matrix can remarkably improve their physical hardness, toughness and oxidation resistance [15, 16]. However, a higher amount of Si-content results in lowering the crystallinity by forming the amorphous silicon nitride (Ni_3N_4) phase [14].

The transition metal nitride based coatings are considered as potential candidates to be used in solar selective surface applications due to a good combination of chemical-, corrosion-, oxidation-, and wear resistance behaviours, extraordinary thermal stability and tuneable optical properties *e.g.*, refractive index, absorptance, reflectance and transmittance; [17-20]. Despite their technological importance, thus far there have been a very limited number of investigations on optical selectivity in the presence of various dopants. For the selective surface applications, these coatings must possess high solar absorption in the visible range and low thermal emittance in the infrared range of the solar spectra. Widespread applications and steadily increasing scientific interests in transition metal nitrides have been dedicated to the development of new thin film composites with superior properties. Properties of nanocomposite transition metal nitrides can be controlled by the type and level of elemental dopant and fabrication procedure. Nanocrystalline transition metal nitrides, carbides and carbonitrides are investigated due to their interesting optical and decorative properties [21-25]. Correlations between chemical structure and optical properties [21, 22, 25], and structural morphology and optical behaviours of CrN, ZrN, TiN systems have been established [21]. Interrelationships among the mechanical properties, chemical composition, optical properties, and crystal structure of DC magnetron sputtered metal nitride thin film coatings was investigated by Zeman *et al*. [26]. Nanocrystalline titanium nitride thin films have applications in different areas of semiconductor device technology *e.g.*, gate electrodes in field-effect transistors, Al diffusion barriers, and ultra-large scale integrated circuits [27-29]. The electronic properties of titanium nitrides and carbides have been extensively studied under different experimental and theoretical approaches [30-34], however optical studies of these materials has not received significant concentration either experimentally or theoretically [30, 35, 36], especially the solar selectivity studies are quite rare [37-43].

The optical analysis of solid materials is very important in order to understand their fundamental characteristics, find their preferable device applications, and identifying other potential zones in which they would demonstrate higher competence. Furthermore, from the simple dispersion relation of refractive index of a solid material, the oscillator energy E_0, dispersion energy parameter E_d, the refractive index at zero photon energy n_0, dielectric constant at high frequency ε_∞, the oscillator position λ_0, the oscillator strength S_0, and loss tangent, volume and surface energy losses are calculated. To date, there has been much scientific articles that have expounded the correspondence between electronic structure and phase stability of metal nitride based films [44, 45]. Transition metal nitride based thin film

coatings also have been found their prospective applications as high temperature structural materials and gate dielectrics in microstructural devices [46]. Meanwhile, attempts at producing new doping materials and research on improving their unique properties are still ongoing [47]. To the best of our knowledge, comprehensive studies on optical and dispersion analysis of transition metal nitride based thin film materials have not been carried out. In view of these issues, in this paper we intend to build up a systematic theoretical background in studying the optical, electronic and dielectric behaviors of transition metal nitride based thin film coating together with a focus onto the recent development of such thin film composites for the applications of solar selective surfaces. Thus, we submit that this review work would provide substantial theoretical aspects and some recent experimental data on the solar selectivity values of transition metal nitride based thin film coatings and assist researchers to carry out research in this field.

2. Optical properties of materials

The optical properties of a material are the responses after being exposed to the electromagnetic spectrum of solar radiation. When a solar radiation is incident upon a material's surface, electromagnetic radiation may be reflected back, refracted through the material, absorbed by the material, transmitted through the materials, scattered by atoms and molecules, and so on. Interactions of light with matters predominantly depend upon the frequency of the incident radiation and the characteristics of the atoms in the materials. In the subsequent sections, we introduce some fundamental optical parameters, theories, principles and concepts associated with the behaviors of electromagnetic radiation and their interactions with materials.

2.1 Optical parameters

Upon the incidence and interactions of solar (or electromagnetic) radiation onto the surface of an object, depending on the energy of the incident photon and nature of the atoms of the material, a large number of various phenomena could arise. In the following sections, we discuss some of the specific optical parameters within the scope of this study.

2.1.1 Optical reflection

When a light exposes on the surface of matter (or boundary between two media), it will return back into the medium at which it has originated from. The reflection of light depends

on the nature of the interface, such as refractive index and surface roughness. Generally, reflection of light arises whenever light passes through the interface of two media having two different refractive indices and level of surface roughness. It is to be noted that a small fraction of the incident light is reflected from the interface while the rest is refracted through the surface into the medium. Reflection of light obeys the following rules:

i. The incident beam, reflected beam and the normal to the reflection surface all lie in the plane of incidence.
ii. The angle of incidence must be equal to the angle of reflection.

Reflectivity or reflectance is also defined as the fraction of the incident light that is reflected at the interface. In mathematical form it is expressed as,

$$R = \frac{I_R}{I_0} \tag{1}$$

where I_0 and I_R are the intensities of the incident and reflected light respectively. In the case of normal incidence, the reflectivity is measured by Fresnel's equation

$$R = \frac{(n_2 - n_1)^2}{(n_2 + n_1)^2} \tag{2}$$

where n_1 and n_2 are the indices of reflection of two media. However, if the incident beam is not perpendicular to the interface, *R* will be a function of the angle of incidence. Since the index of reflection of air is near about unity, hence when light travels from air into a solid medium the reflectivity is given as,

$$R = \frac{(n_1 - 1)^2}{(n_s + 1)^2} \tag{3}$$

This states that the higher the index of refraction of the solid medium, the greater is the reflectivity. Since the refractive index of a solid material depends on the incident beam's wavelength, the reflectivity also varies with the wavelength.

2.1.2 Optical refraction and refractive index

Two optical constants: refractive index (*n*) and the extinction coefficient (*k*) are conveniently used to represent the propagation electromagnetic waves and their dissipation of energy in the medium of propagation. Assuming the material to extend indefinitely, the complex refractive index can be defined by the following function [48],

$$\widetilde{N} = n + ik = \left[\epsilon\mu + i\frac{4\pi\mu\sigma}{\omega}\right]^{\frac{1}{2}}$$

$$= \left[\mu(\epsilon + i\frac{4\pi\sigma}{\omega})\right]^{\frac{1}{2}}$$

$$= [\mu\tilde{\epsilon}]^{\frac{1}{2}} \quad (4)$$

Complex wave vector,

$$\bar{q} = \frac{\omega}{c}\,\tilde{N}$$

$$= \frac{n\omega}{c} + i\,\frac{k\omega}{c} \quad (5)$$

where the refractive index n and the extinction coefficient k are defined in terms of by the conductivity (σ_1), the permeability (μ_1), and the dielectric constant (ϵ_1):

$$n^2 = \frac{\mu}{2}\left[\left\{\varepsilon^2 + \left(\frac{4\pi\sigma}{\omega}\right)^2\right\}^{1/2} + \epsilon\right] \quad (6)$$

$$k^2 = \frac{\mu}{2}\left[\left\{\varepsilon^2 + \left(\frac{4\pi\sigma}{\omega}\right)^2\right\}^{1/2} - \epsilon\right] \quad (7)$$

Equations (6) and (7) contain information on the propagation of the electromagnetic waves in the matter. The quantities ϵ, σ and μ are defined only when $\omega = 0$. Thus, in terms of n and k the dielectric constant, permeability and conductivity are expressed:

$$n^2 - k^2 = \epsilon\mu \quad (8)$$

$$2nk = \frac{4\pi\mu\sigma}{\omega} \quad (9)$$

Thus, Eq. (4) can be rearranged as [48],

$$\tilde{N}^2 = \left[\mu\left(\epsilon + i\frac{4\pi\sigma}{\omega}\right)\right] = \mu\tilde{\epsilon} \approx \frac{4\pi i\mu\tilde{\sigma}}{\omega} \quad (10)$$

The absolute value of $\tilde{N}$ and the phase difference ϕ between the magnetic and dielectric field vectors are given by,

$$\left|\tilde{N}\right| = (n^2 + k^2)^{\frac{1}{2}} \quad (11)$$

$$tan\phi = \frac{k}{n} \quad (12)$$

In an ideal insulator or in free space, the electric and magnetic fields are in phase because $k = 0$. However in a metal at low frequencies, $n \approx k$ and phase difference $\phi = 45°$.

2.1.3 Optical scattering

In general, scattering is a physical process at which various types of waves (light, sound etc) or particles are deviated from their straight trajectory due to some localized irregularities in the medium they pass through or at the interface between two media. Scattering may arise due to the physical collision between electrons, protons, atoms, molecules, photon and other

kinds of particles. Absorption and scattering are two major physical processes that contribute to the visible appearance of most objects. An object is identified as white because of its appearance to multiple scattering of light by internal or surface inhomogeneity. An effective scattering surface is dusty, dull or without a sheen whereas a surface which doesn't permit scattering has a refined and glossy appearance. Scattering in light can be caused via two mechanisms: surface scattering and volume scattering. Surface scattering emerges from the interaction of photons of light with the surface of a material while the volume scattering occurs only in the bulk of the material and is completely independent of the surfaces of the material. Surface scattering of light is a consequence of the interaction of light photons with the electric filed of a particle or molecule of a material. The incident photons induce oscillating dipoles around the electron cloud and radiate energy in all possible directions. This radiated energy is called the scattering of light. Scattering of light by individual particles depends on the particle's size, refractive index and the wavelength of the incident light.

2.1.4 Optical absorptance and optical emittance

Solar radiation on a non-metallic material can be absorbed *via* two mechanisms: electronic polarization and valence band-conduction band electron transitions. The first kind of absorption is only important at light frequencies around the relaxation frequency of the constituent atoms, while the other mechanism involves valence band-conduction band electron transitions that depend upon band-gap, and band structures. When a solar radiation impinges upon the surface of a material, it is absorbed by the excitation of an electron from the nearly filled valence band, across the band gap, and into an empty state within the conduction band. This phenomenon has been described in the following Figure 1. As a result, a free electron is created in the conduction band leaving a hole behind the valence band. Absorption of light photon satisfies the following relationship,

$$h\nu \geq E_g \tag{13}$$

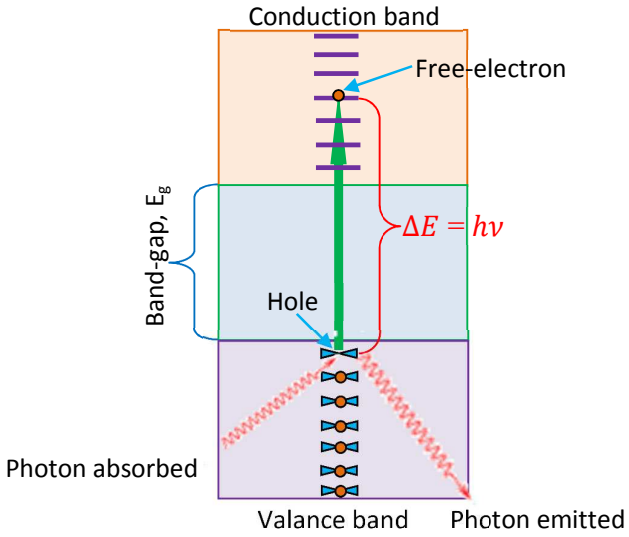

Figure 1. Phenomenon of photon absorption in a material.

In terms of wavelength, Eq. (13) can be written as,

$$\frac{hc}{\lambda} \geq E_g \tag{14}$$

Maximum and minimum band-gap energy at which light is absorbed in a material can be computed using the following two respective equations:

$$E_g(\max) = \frac{hc}{\lambda_{min}} \tag{15}$$

$$E_g(\min) = \frac{hc}{\lambda_{max}} \tag{16}$$

However, the intensity of the absorbed solar radiation depends on the nature of the medium and exponentially decreases with distance traversed by the light according to the following relation,

$$I = I_0 e^{-\beta x} \tag{17}$$

where x is the intensity of the incident radiation and β is the absorption coefficient, characteristic of the particular material. Materials that possess large β are highly absorptive. Upon the incidence of solar radiation into the surface of a material, some part of the light is absorbed, some portion is reflected back to the medium while the rest being transmitted through the material are demonstrated in the following Figure 2.

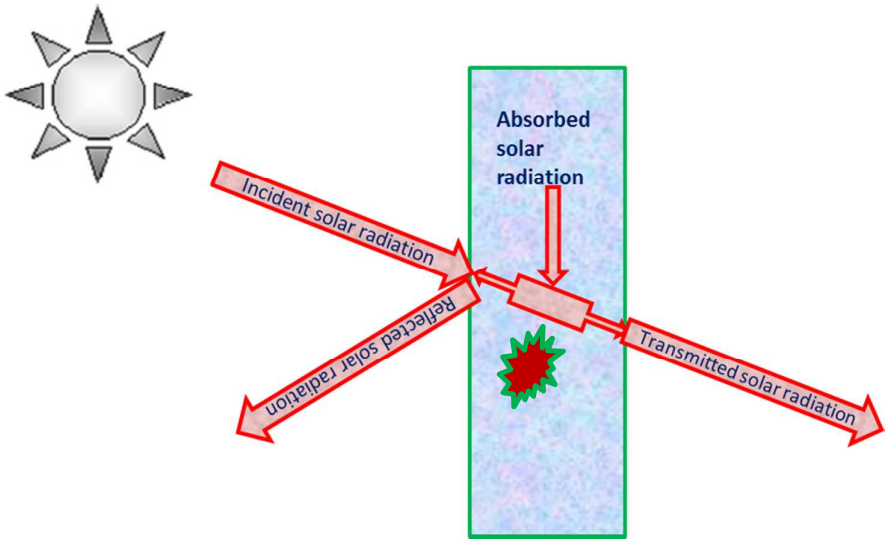

Figure 2. Phenomenon of absorption, reflection and transmission of solar radiation.

For a certain incoming solar radiation; the solar absorptance, reflectance and transmittance can be expressed by the following relationship,

$$\alpha(\lambda) + \rho(\lambda) + t(\lambda) = 1 \quad (18)$$

Generally, for a highly reflecting metal or opaque surface, the transmission coefficient is zero *i.e.*, $t(\lambda) = 0$, and energy is absorbed or reflected from all directions. Hence, the solar absorptance becomes equal to the solar emittance,

$$\alpha(\lambda) = \varepsilon(\lambda) = 1 - \rho(\lambda) \quad (19)$$

The solar absorptance of a material's surface is defined as a fraction of solar radiation incident on the surface of the material that is absorbed. The solar absorptance is a function of both the incident spectrum and the reflection function of the material. From Eq. (19), the solar absorptance and solar emittance of any material can be conveniently computed *via* Duffie and Beckman method using the following relationships Equations (20) and (22) [49, 50],

$$\alpha = \frac{\int_0^\infty I_s(\lambda)(1-\rho(\lambda))d\lambda}{\int_0^\infty I_s(\lambda)d\lambda} \quad (20)$$

Here $(1 - \rho(\lambda))$ is the absorbed light, where $\rho(\lambda)$ is the measured reflection as a function of the wavelength λ and I_s is the intensity distribution of the incoming solar radiation. The solar spectrum has an air mass of AM1.5 in accordance with the ISO standard 9845-1 (1992).

In the solar absorption process of solar selective coatings, the valence electrons absorb energy from the sunlight and jump into the conduction bands. But the essential condition is specified

in Eq. (14) (*i.e*., the energy of photons must be equal to greater less than the gap of forbidden energy band). Generally, the transition metals Cr, Mn, Ni, Mo, *etc*. have excellent forbidden energy gaps, and after the introduction of various doping (oxide or nitride or oxynitride) they become outstanding absorbing materials.

The spectral of a blackbody is temperature dependent. The solar emittance is defined as the weighted fraction (by total power density) of the emitted radiation and can be calculated using the intensity distribution of a blackbody spectrum within the operating temperature of the absorbing medium. For high temperature applications, this is generally regarded as being greater than 400 °C. The operating temperature is estimated as the temperature at which the solar absorptance becomes equal to the solar emittance and temperature attains static equilibrium. Thus, the equilibrium temperature can be computed according to the well-known Stefan-Boltzmann law:

$$T = 4\sqrt{\left(\frac{S\alpha}{4\varepsilon\sigma}\right)} \tag{21}$$

where S is the solar constant and σ is the Stefan-Boltzmann's constant. From Eq. (19), the solar emittance of any material can be estimated *via* Duffie and Beckman method [49, 50],

$$\varepsilon(T) = \frac{\int_0^\infty I_p(\lambda)(1-\rho(\lambda))d\lambda}{\int_0^\infty I_p(\lambda)d\lambda} \tag{22}$$

where I_p is the intensity distribution of the Planck black-body.

The solar absorptance and thermal emittance are material-dependent parameters that can be estimated from optical measurements.

2.1.5 Solar selectivity

Generally, an ideal solar selective surface would have zero reflectance in the visible range of the solar spectrum and 100% reflectance in the infrared region of the solar spectrum which corresponds to the thermal radiation spectrum of a blackbody at the operating temperature of the absorbing surface. In real life, no such ideally selective surface exists that absorbs 100% of the incident solar radiation in the visible range and reflects 100% of the incident solar radiation in the IR range. However, in the laboratory we can fabricate solar selective materials that can maximise the solar absorption in the visible range and minimise the energy lost *via* thermal emittance. A very common way of preparing a solar selective surface is to apply a highly solar absorptive thin film onto a non-selective highly reflective metal substrate

which is generally known as absorber–reflector tandem system. Absorption, transmission and emission from such an absorber–reflector tandem system are depicted in Figure 2. The spectral features of an ideal solar selective surface and the basis of a real solar selective surface are clearly demonstrated in Figure 3 [51]. At earth's surface, the incident solar flux is limited to the range between 0.3 and 2.5 μm (in the UV-Vis-NIR wavelength range) with the maximum solar intensity at 0.55 mm. In the infrared and far-infrared (IR-FIR) range of the solar spectrum, the optical response of a real material can be characterized by its thermal emission compared to an ideal blackbody at 100, 200 and 300 °C. Figure 3 indicates that, as the temperature of the blackbody increases, energy emission increases and the peak positions move towards the shorter wavelengths of the spectrum. These features indicate the potential of patterning a material that absorbs the maximum amount of incident solar radiation and reemits a minimum amount of the absorbed radiation. This is the fundamental concept of forming an ideal solar selective surface. The performance criterion of a solar selective surface is, generally, evaluated by the ratio of the solar absorptance (α) to the thermal emittance (ε) via following relation,

$$s = \frac{\alpha}{\varepsilon} \tag{23}$$

This important parameter, s is known as the solar selectivity of the solar selective surface.

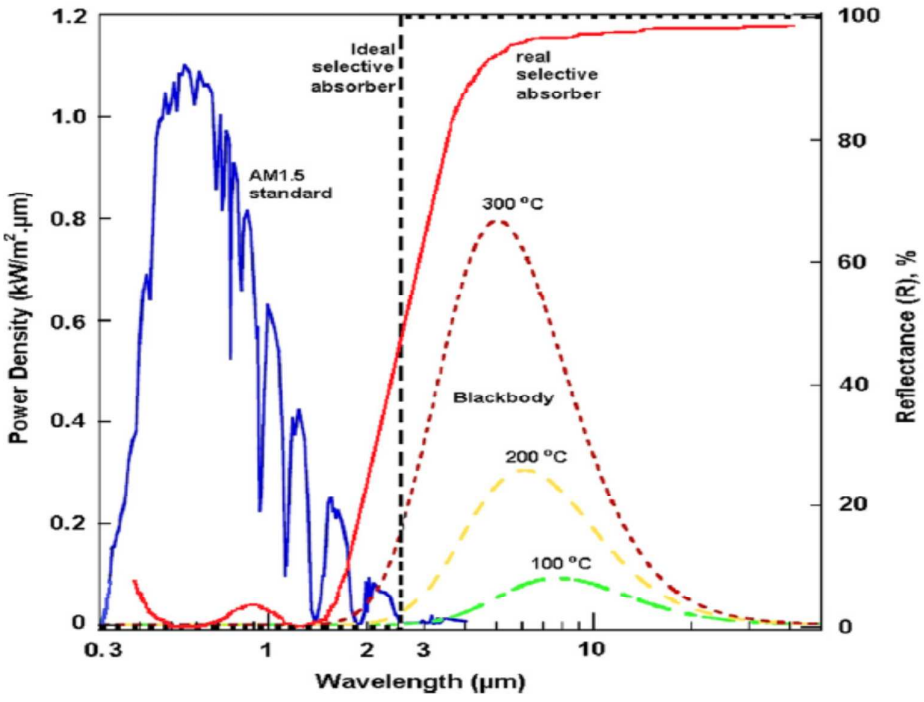

Figure 3. Spectral features of an ideal and real solar selective surface, the solar spectrum at AM 1.5 (ISO standard 9845-1 (1992)) and the blackbody-like emission spectra at temperatures 100, 200 and 300 °C. Reprinted with permission from Ref. [51].

In a typical solar thermal conversion system, the sunlight is strongly absorbed as heat at the absorbing surface and a small portion of the incident solar radiation is lost to the environment *via* convection and radiation. A spectrally selective absorbing surface based on cermet is composed of ceramics and metal components. An effective spectrally selective surface can be formed by integrating with an antireflection coating (ARC) and an infrared-reflective base layer as depicted in the following Figure 4.

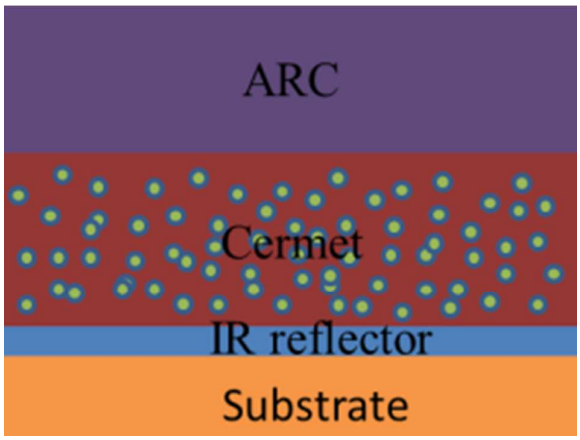

Figure 4. The anti-reflection coating (ARC) helps to reduce solar reflection off the surface; the cermet provides solar absorption; and the IR reflector (*e.g.*, Cu, Al, Mo, or other metal with low intrinsic emissivity) aids to decrease the radiation losses. The substrate can be either a metal or a glass. Reprinted with permission from Ref. [52].

Double cermets based selective solar coatings can be deposited onto metal (stainless steel, SS) or glass substrates using sputtering system. A multilayer film was deposited on flexible metal or glass substrates: from the bottom side, a Mo IR reflector layer, a high metal volume fraction (HMVF) metal oxide layer, a low metal volume fraction (LMVF) layer, and an antireflection coating on the top of film surface (see Figure 5) [53]. Another similar type of solar selective design has been proposed elsewhere [54]. Each layer deposited onto glass and

stainless steel substrates in order to successive measure of the film thickness, reflectance, and transmittance, respectively.

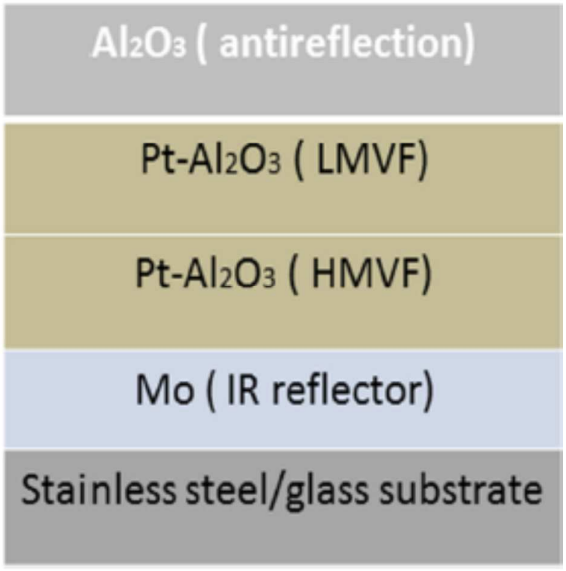

Figure 5. Solar selective designs of cermet based solar selective surface. Reprinted with permission from Ref. [53].

In a cermet based solar selective coating, metal component is surrounded in the dielectric matrix by a metal oxide, metal nitride, or metal oxynitride constituents. A cermet shows ceramic behaviors in the visible range of the solar spectrum and metallic properties in the infrared spectrum. The film thickness, constituents, particle size, surface morphology, crystalline orientation, and metal volume fraction in the matrix, strongly affect the ceramic and metallic properties exhibited across the visible and infrared spectra. Higher film thickness and reduced particle sizes are favorable for higher solar absorptance, while an increase in particle radius results in an alteration of the solar absorption and scattering, and thereby causing a lower absorption in the visible spectra. Furthermore, the thermal emittance in the infrared range can be decreased by reducing the film thickness and increasing the metal volume fraction [55]. In general, smaller size particles are influenced by the interference phenomena and are more sensitive to thickness changes. Thus, the desired optical properties of the cermet based solar selective coatings can be achieved by optimizing the film thickness and particle diameter.

The microstructure and spectral selectivity of a series of thin films based solar selective cermets coating integrated with Al_2O_3 antireflection layer, as depicted in Figure 5, exhibited

high solar absorptance of 0.92 and a relatively low thermal emittance of 0.19 at 80 ^{o}C [56]. However, after thermal treatment of the films at 800 ^{o}C for 2 hours in vacuum, the solar absorptance dwindled to 0.91 and the thermal emittance attained to 0.27. It is suspected that after such thermal treatment, some defects such as widened the grain boundaries, cracks and holes were initiated around the Al_2O_3 layer, which induced the Mo diffusion, and decreased the spectral selectivity values of the deposited coatings. During the high temperature annealing, the microstructure of solar selective coatings is changed which also plays an important role in altering the solar selectivity behaviors because grain size of the coatings is diligently associated with the optical properties. As the grain size is decreased, the scattering of the ultraviolet light (within the range of 300-400 nm) gets stronger and thereby reduce the reflectance.

The solar absorptance for AlCrON coatings increased and the grain size decreased, after thermal treatment at 500 °C in air [57]. In another study, Zheng *et al*. [58] reported that vacuum annealing at 600 °C causes the refinement of Mo grains, forming a denser and compact cermet layer. Consequently, the solar thermal conversion efficiency was increased by 0.6%, however at 800 °C this resulted to the anomalous growth of Mo grains, and a decrement of the solar thermal conversion efficiency by 1.3%. This reveals the fact that the grain boundaries and interfaces have excess energy after synthesis of the films, and the minimization of the total energy delivers a driving force of the grain size refinements. It is thought that, with the increase of heat treatment duration, the residual stress will release *via* boundary diffusions or atomic movements, and thus enables the grain size refinements. Apart from abnormal grain size refinements, there exist many other defects that intensely impact the various properties of solar selective coatings, such as widened interface, presence of water molecules, oxidations, presence of cavity, and cracks.

2.2 Other optical properties

Generally, optical studies of materials are predominantly based on the transmittance and/or the reflectance measurements in the UV-visible range of the solar spectra. Using the UV-visible transmittance and/or the reflectance spectra, a number of other optical parameters can be estimated which provide substantial information on structural, optical and electronic mechanisms occurring in these materials, and their fundamental characteristics . In the

subsequent sections of this review article, we describe a large number of optical and dielectric properties of solid materials which will be useful for materials researchers.

The optical band structure and the types of electron transition involved in the absorption process of thin film coatings and other materials can be identified from the linear absorption coefficient [59, 60],

$$\beta = 2.3026 \frac{A}{d} \quad (24)$$

where β is the absorption coefficient, A is the solar absorptance assessed from the UV-Vis reflectance data, and d is the thickness of the films.

In the crystalline and other materials the optical energy gap, E_g and the electron transition type can be estimated from the absorption coefficient and optical absorption edge using Tauc relation [49, 61, 62],

$$\beta h\nu = C(h\nu - E_g)^x \quad (25)$$

where, β is the absorption coefficient, $h\nu$ is the incident photon energy, h is Planck's constant, ν is the frequency of incident light, C is an energy independent constant, E_g is the optical band-gap and x has a value of either $\frac{1}{2}$ or 2 for the direct and indirect optical transitions, respectively. The direct energy band-gap is estimated by plotting $h\nu$ vs $(\alpha h\nu)^2$ and extrapolating the linear portion of the curve to $(\alpha h\nu)^2 = 0$ along the x-axis while the indirect band-gap can be computed by plotting $h\nu$ vs $(\alpha h\nu)^{1/2}$ and extrapolating the linear part of the curve to $(\alpha h\nu)^{1/2} = 0$ along $h\nu$-axis.

Since the solar absorption in a material depends on the existence of localized states in the forbidden energy band-gap, the solar absorption spectra can provide with the significant information about the localized states and the occurrence of disorderness in the material. Below the optical band-gap, the absorption coefficient shows an exponential decline by forming so-called Urbach tails, and is expressed as,

$$\beta(h\nu) = \beta_0 e^{\left(\frac{h\nu}{E_u}\right)} \quad (26)$$

where β_0 is a constant and E_u is the Urbach energy indicates the widths of optical absorption edges. Equation (3) can be rearranged as,

$$\beta = \beta_0 \exp\left(\frac{\gamma h\nu}{k_B T}\right) \quad (27)$$

where γ is the steepness parameter denoting the broadening of absorption edges and expressed as,

$$\gamma = \frac{k_B T}{E_u} \tag{28}$$

The complex refractive index, used to interpret many other properties of thin film materials and their derivatives is, defined as,

$$n^* = n + ik \tag{29}$$

where n is real, and k is the imaginary part of the complex refractive index known as the extinction coefficient which can be directly estimated from the known value of α *via* following relation,

$$k = \frac{\alpha\lambda}{4\pi} \tag{30}$$

The refractive index, n is defines as,

$$n = \left(\frac{1+R}{1-R}\right) + \sqrt{\frac{4R}{(1-R)^2} - k^2} \tag{31}$$

where R is the reflectance in percentages, and k is the well-known extinction coefficient.

The phenomenon of optical dispersion plays an important role in optical communication and in the design of optical devices. Using DiDomenico *et al.*'s single oscillator model [63], the relationship for the dispersion of refractive index below the energy band-gap of a material is represented as,

$$(n^2 - 1)^{-1} = \frac{E_0}{E_d} - \frac{1}{E_0 E_d}(h\nu)^2 \tag{32}$$

where E_d is the dispersion energy indicating the strength of optical transition and E_0 is the single oscillator energy. The values of dispersion energy parameters can be calculated from the intercept of a straight line drawn between $(\mu^2\text{-}1)^{-1}$ and $(h\nu)^2$ to $(\mu^2\text{-}1)^{-1}$ axis, (E_0/E_d) and the gradient/slope $(E_0E_d)^{-1}$. The optical dispersion energy parameters E_0 and E_d also depend on the optical transition moments M_{-1} and M_{-3} by the following equations [64],

$$E_0^2 = \frac{M_{-1}}{M_{-3}} \text{ and } E_d^2 = \frac{M_{-1}^3}{M_{-3}} \tag{33}$$

The strength of oscillator energy, E_0 and dispersion energy, E_d values are also related to the crystalline structure and ionicity of ionic or covalent materials which reveals that in addition to the optical properties, the single oscillator model can be applied to gain the structural information of a material [65]. The oscillator strength, f is defined by Wemple and DiDomenico single oscillator model is given by [63],

$$f = E_0 E_d \quad (34)$$

The high frequency optical dielectric constant, ε_∞ known as static dielectric constant, and the static refractive index, n_0 is associated with the oscillator energy, E_0 and dispersion energy, E_d by the following relation [64],

$$n_0^2 = \varepsilon_\infty = 1 + \frac{E_d}{E_0} \quad (35)$$

In the longer wavelength regions, the dispersion of refractive index is expressed in terms of Sellemeier relation [64, 66, 67],

$$\frac{n_0^2-1}{n^2-1} = 1 - \left(\frac{\lambda_0}{\lambda}\right)^2 \quad (36)$$

where λ_0 is the average inter-band oscillator wavelength and n_0 is the refractive index at zero photon energy. Equation (14) can be re-ordered to,

$$n^2 - 1 = \frac{S_0 \lambda_0^2}{1-\frac{\lambda_0^2}{\lambda^2}} \quad (37)$$

where S_0 is the average oscillator strength related to the inter-band oscillator wavelength and static dielectric constant by the following relation [66, 67],

$$S_0 = \frac{n_0^2-1}{\lambda_0^2} \quad (38)$$

The complex dielectric function of solid materials can be defined using the dispersion relation of the incident photon,

$$\varepsilon(\omega) = \varepsilon_1(\omega) + i\varepsilon_2(\omega) = \big(n(\omega) + ik(\omega)\big)^2 \quad (39)$$

where ε_1 and ε_2 are the real and imaginary parts of the complex dielectric constant, respectively are correlated to the refractive index and extinction coefficient as [66],

$$\varepsilon_1 = n^2 - k^2 \text{ and } \varepsilon_2 = 2nk \quad (40)$$

Since below the optical band-gap energy, the free carrier absorption play a significant role in the absorption process thus, the real part of dielectric constant, ε_1 must include the carrier contribution and take the following relation [68],

$$\varepsilon_1 = n^2 - k^2 = \varepsilon_\infty - \left(\frac{Ne^2}{4\pi^2 c^2 \varepsilon_0 m^*}\right)\lambda^2 \quad (41)$$

While the imaginary part of the dielectric constant, ε_2 will be written as,

$$\varepsilon_2 = 2nk = \left(\frac{\varepsilon_\infty \omega_p^2}{8\pi^2 c^3 \tau}\right)\lambda^3 \quad (42)$$

where ε_∞ is the dielectric constant at high frequency, e is the electron's charge, c is the speed of light, ε_0 is the permittivity of free space, N is the free carrier concentration, m^* is the

effective mass, ω_p is the plasma frequency, τ is the relaxation time and k is the extinction coefficient. The ε_1 and ε_2 represent the quantity of energy deposited in dielectrics as polarization and energy loss, respectively. In solid materials, power loss in the form of heat is known as loss tangent, and is normally associated with the inelastic scattering in charge transfer and charge conduction processes during device operations. Mathematically, the loss tangent is defined as,

$$tan\delta = \frac{\varepsilon_2}{\varepsilon_1} \tag{43}$$

It measures the loss-rate of power in a mechanical and oscillatory dissipative system. This power loss is related to the fact that dipole alignments become insignificant at lower temperatures however, at higher temperatures the orientations of dipoles are governed by the thermal excitements and thereby the power loss is enhanced.

In dielectric materials, the inelastic scattering of electrons is associated with energy loss functions known as volume energy loss function, V_{el} and surface energy loss function, S_{el} [66].

$$V_{el} = Im\left(-\frac{1}{\varepsilon(\omega)}\right) = \frac{\varepsilon_2}{\varepsilon_1^2 + \varepsilon_2^2} \tag{44}$$

$$S_{el} = Im\left(-\frac{1}{\varepsilon(\omega)+1}\right) = \frac{\varepsilon_2}{(1+\varepsilon_1)^2 + \varepsilon_2^2} \tag{45}$$

As seen from Equations (44) and (45), the energy loss functions are connected to the optical characteristics of a material by its real and imaginary parts of dielectric function.

The dielectric relaxation time, τ is defined by the following relation [69],

$$\tau = \frac{\varepsilon_\infty - \varepsilon_1}{\omega\varepsilon_2} \tag{46}$$

where ε_∞ is the dielectric constant at high frequency, and ε_1 and ε_2 are the real and imaginary parts of the dielectric functions, respectively.

The optical absorption coefficient, β is used to estimate the optical conductivity of solid materials as follows,

$$\sigma_{opt} = \frac{\beta nc}{4\pi} \tag{47}$$

where n is the refractive index and c is the speed of light.

3. Real-life applications of transition metal nitride/oxynitride based coatings: spectral selectivity data of recently developed materials

The optical applications of metal nitrides based selective solar coatings have been extensively discussed in a previous review study [70]. In Ref. [42], magnetron sputtered TiAlN/TiAlON coatings synthesized onto a metal substrate demonstrated high solar absorptance in the visible range and low thermal emittance in the infrared range. The solar absorptance of TiAlN/TiAlON coatings was substantially enhanced to 0.95 by coated with Si_3N_4 antireflection layers on the top of these films. A high thermal stability in air up to 600 °C and high solar selectivity of 0.95/0.07 = 13.57 was achieved. Since, solar selective surfaces are the easiest and most direct way to enhance the solar energy harvesting of solar energy captors, in recent years, transition metal nitrides have received significant research interest for middle (up to 200 °C) and high temperature (Up to 600 °C) solar applications [18, 19, 42, 71-79]. The solar selectivity values of some recently published transition metal nitride/oxynitride based thin film coatings are listed in Table 1.

Table 1. Spectral selectivity values of transition metal nitride/oxynitride based thin film coatings as seen in the literature.

Sample compositions	Substrate	Absorptance (α) and emittance (ε) calculation method	Solar selectivity, $s = \frac{\alpha}{\varepsilon}$
TiN	Stainless steel	UV-Vis and FTIR reflectivity	8.48 [62]
TiAlN	Stainless steel	UV-Vis and FTIR reflectivity	12.92 [62]
TiAlSiN	Stainless steel	UV-Vis and FTIR reflectivity	22.63 [62]
TiAlSiN	Stainless steel	UV-Vis and FTIR reflectivity	22.63-24.63 [50]
TiAlN	Copper	Solar spectrum reflectometer and emissometer	12.9 [80]
TiAlN/TiAlON	Copper	Solar spectrum reflectometer and emissometer	15.2 [80]
$Ti_{1-x}Al_xN$	Copper	UV-Vis and FTIR reflectivity	For x = 0.21; 5.4 [81]
	Copper	UV-Vis and FTIR reflectivity	For x = 0.58; 5.0 [81]
TiAlN/TiAlON/Si_3N_4	Copper	Solar spectrum reflectometer and emissometer	13.6 [42, 80, 82]
TiAlN/TiAlON/Si_3N_4	Glass	Solar spectrum reflectometer	13.3 [80]

		and emissometer	
$TiAlN/TiAlON/Si_3N_4$	Stainless steel	Solar spectrum reflectometer and emissometer	7.4 [80]
$TiAlN/TiAlON/Si_3N_4$	Nickel	Solar spectrum reflectometer and emissometer	6.7 [80]
$Ti_{1-x}Al_xN/Ag/ Ti_{1-x}Al_xN$	Glass	UV-Vis and FTIR reflectivity	18.1 [83]
$Ti_{0.5}Al_{0.5}N/ Ti_{0.25}Al_{0.75}N/AlN$	Stainless steel	Spectroscopic phase modulated ellipsometer	23.5 [84]
$Ti_xAl_{1-x}/(TiN\text{-}AlN)_H/(TiN\text{-}AlN)_L/AlN$	Stainless steel	UV-Vis-NIR and emissometer	11.8 [85]
TiAl/TiAlN/TiAlON/TiAlO	Stainless steel and Copper	Spectrophotometer and FTIR	11.3 [86]
TiN/Al_2O_3	Stainless steel	UV-Vis-NIR and FTIR spectroscopies	8.36 [87]
$Cu/Zr_{0.2}AlN_{0.8}/ZrN/AlN/ZrN/AlN/Al_{34}O_{62}N_4$	Si(1 11) and glass (soda lime glass)	UV-Vis-NIR and FTIR spectroscopies	7.85 [88]
$TiAlN/SiO_2$	Copper and Silicon	UV-Vis-NIR and FTIR spectroscopies	15.33 [89]
TiAlC/TiAlCN/TiAlSiCN/TiAlSiCO/TiAlSiO	Stainless steel	UV–vis–NIR spectrophotometer	6.4 [90]
$CrON/SnO_2$	Aluminium	UV-Vis-NIR and FTIR spectroscopies	19.00 [91]
CrN/Si_3N_4	Aluminium	UV-Vis-NIR and FTIR spectroscopies	15.49 [91]
CrN/SiO_2	Aluminium	UV-Vis-NIR and FTIR spectroscopies	15.11 [91]
$WAlN/WAlON/Al_2O_3$	Stainless steel	UV-Vis-NIR and FTIR spectroscopies	11.98 [92]
$CrN(H)/CrN(L)/CrON/Al_2O_3$	Stainless steel	UV-Vis-NIR and FTIR spectroscopies	6.64 [93]
$ZrO_x/ZrC\text{-}ZrN/Zr$	Stainless steel and Copper	UV-Vis-NIR and FTIR spectroscopies	22.00 [94]
$HfMoN(H)/HfMoN(L)/HfON/Al_2O_3$	Stainless steel	UV-Vis spectrometer and emissometer	6.79 [95]

$CrAlN/CrAlON/Al_2O_3$	Copper	Solar spectrum reflectometer and emissometer	14.06 [96]
$CrAlN/CrAlON/Si_3N_4$	Copper	Solar spectrum reflectometer and emissometer	11.5 [96]
$TiAlN/TiAlON/Si_3N_4$	Metal and non-metal	Phase modulated spectroscopic ellipsometry	11.5 [42]
Cu/NbAlN	Copper	Phase-modulated spectroscopic ellipsometer	15.68 [72]
Cu/NbAlN/NbAlON	Copper	Phase-modulated spectroscopic ellipsometer	15.50 [72]
$Cu/NbAlN/NbAlON/Si_3N_4$	Copper	Phase-modulated spectroscopic ellipsometer	13.66 [72]
Ti/AlTiN/AlTiON/AlTiO	Stainless steel	UV-Vis-NIR and FTIR spectroscopies	11.94 [97]
Al-AlN	Aluminium	UV-Vis-NIR and FTIR spectroscopies	14.27 [98]
$TiAlSiN/TiAlSiON/SiO_2$	Copper	UV-Vis-NIR and FTIR spectroscopies	10.93 [99]
$Al/NbMoN/NbMoON/SiO_2$	Stainless steel	UV-Vis-NIR and FTIR spectroscopies	8.62 [100]
TiAlC/TiAlCN/TiAlSiCN/ TiAlSiCO/ TiAlSiO	Stainless steel	UV-Vis-NIR and FTIR spectroscopies	6.41 [101]
$TiAlN_x/TiAlN_y/Al_2O_3$	Stainless steel	UV-Vis-NIR and FTIR spectroscopies	4.23 [102]
$Al/Si_3N_4/(Ti/Si_3N_4)^2$	Silicon	UV-Vis and frontier spectroscopies	13.43 [103]
$Mo/ZrSiN/ZrSiON/SiO_2$	Stainless steel	UV-Vis-NIR and FTIR spectroscopies	15.67 [104]
Al-AlN	Aluminum metal	A commercial optical software SCOUT	48.00 [105]
TiN_xO_y	Copper	UV-Vis-NIR and FT-NIR/MIR spectroscopies	15.94 [106]

Over the years, transition-metal nitrides and transition-metal oxynitrides based thin film coatings have gained substantial attention for use in mid to high temperature solar selective

surfaces due to a good combination of their physical, chemical, optical and many other properties. The solar selective performance of a large number of recently developed transition-metal nitrides and transition-metal oxynitrides thin film based solar selective surfaces have been presented in Table 1. Higher values of solar selectivity of these thin film based solar selective coatings essentially indicating their high solar absorbance in the visible range and low thermal emittance in the infra-red range of the solar spectra. The solar selective performance of the transition-metal nitrides and transition-metal oxinitrides based coatings can be significantly modified by adjusting the films' stoichiometry that leads to changes in the density of free electrons in the *d*-bands. Some of the typical UV-Vis and FTIR spectra of the aforementioned solar selective surfaces are presented in the following section.

A number of ZrSiN and ZrSiON absorbing layers prepared via magnetron sputtering system in a multi-target assembly onto the glass substrates with different reactive gas flows [104]. A high solar absorptance of 0.94 and a low thermal emittance of 0.06 at 25 °C were achieved [104]. As seen in Figure 6, a wide range of reflectance and transmittance values, for the various absorbing layers, was obtained. It was further noticed that with the subsequent increase in the reactive gas flows the reflectance values decrease and the transmittance values increase which arises due to a transition from metal-like behaviour to dielectric-like behaviour of the absorbing surfaces.

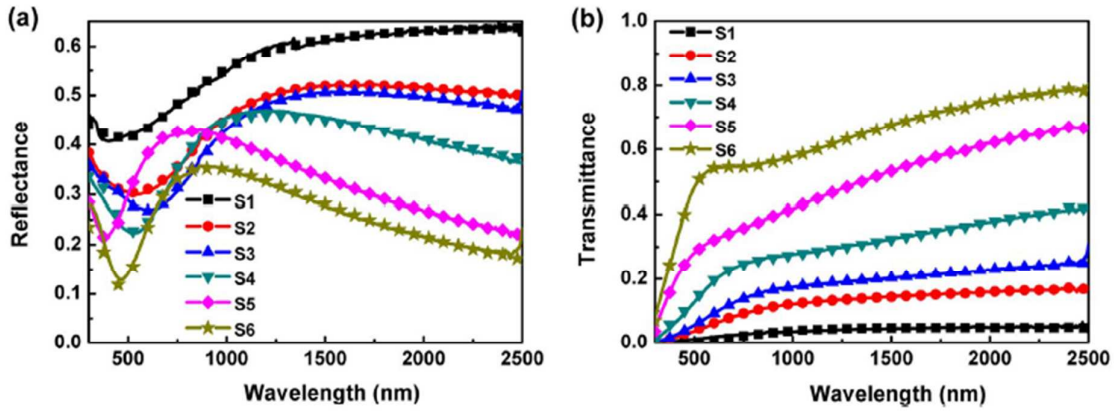

Figure 6. The UV-Vis (a) reflectance and (b) transmittance spectra of ZrSiN (S1, S2, S3) and ZrSiON (S4, S5, S6) solar selective coatings deposited onto glass substrates. Samples S1, S2, S3, S4, S5, and S6 differs in different amount of reactive gas flows and film thickness. Reprinted with permission from Ref. [104].

The Al/NbMoN/NbMoON/SiO_2 solar selective absorbing coatings developed for its potential applications in concentrated solar power (CSP) system were deposited onto the stainless steel substrates *via* magnetron sputtering method [100] (See Figure 7). These coatings show a high value of solar absorptance and higher degree of thermal stability both in air and in vacuum up to 450 °C however, substantial degradation of the optical performance of these coatings was noticed at an annealing temperature of 500°C.

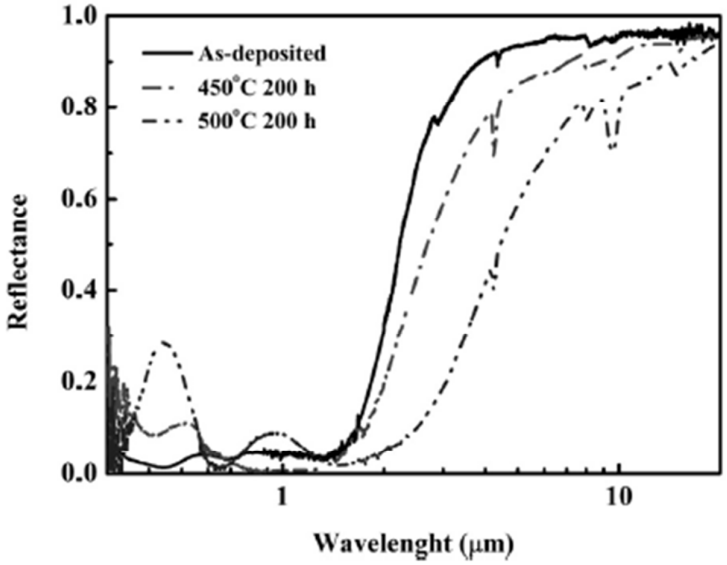

Figure 7. The reflectance spectra of the Al/NbMoN/NbMoON/SiO_2 solar selective absorbing coating before and after being annealed at 450 °C and 500 °C for 200 h in air. Reprinted with permission from Ref. [100].

Figure 8 shows the UV-visible reflectance spectra of as-deposited, 400 ºC and 600 ºC vacuum annealed RF sputtered Mo-Si_3N_4 solar selective coatings [107]. This first annealing was carried out to remove the inert sputtering gas remaining around the coating surfaces responsible to shrink the coating multilayers and modifying the optical interferences. As a result, a higher degree of optical stability was attained by the solar selective coatings after being vacuum annealed at 600 ºC.

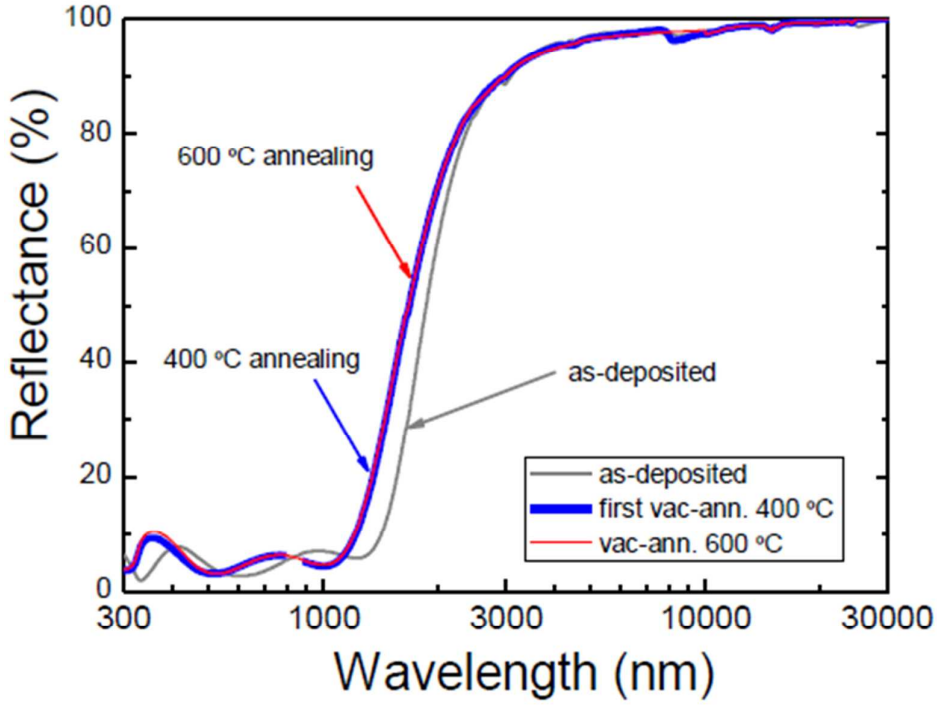

Figure 8. The UV-Vis reflectance spectra of Mo-Si_3N_4 solar selective coatings deposited onto the stainless steel substrates annealed at 400 and 600 °C in vacuum. Reprinted with permission from Ref. [107].

The optical reflectance spectra ((See Figure 9(A)) of TiN, TiAlN and TiAlSiN thin film coatings deposited onto M2 steel substrates via magnetron sputtering technique were used to calculate the solar absorptance [62]. Figure 9 indicates the films have moderate absorptance to ultraviolet region, high absorptance in the visible region and very high reflectance in the near-infrared region of the solar radiation. This means that the highest value of the solar absorption is in the visible range of the solar spectrum and the lowest value of solar absorption is recorded in the near-infrared region. Due to this superior value of the solar absorptance, these films are considered efficient candidates to be used as solar selective surfaces. The FTIR reflectance spectra of these solar selective films shown in Figure 9(B) were used to estimate the thermal emittance values in the infrared range of the solar spectra [62]. The thermal emittance values of these films were decreased with the Al- and AlSi-doping to the TiN matrix. It is believed that as the Al and Si are added to the TiN system, the thermal emittance reduction was governed by the formation of the surface oxidation layers such as Al_2O_3, SiO_2 [62].

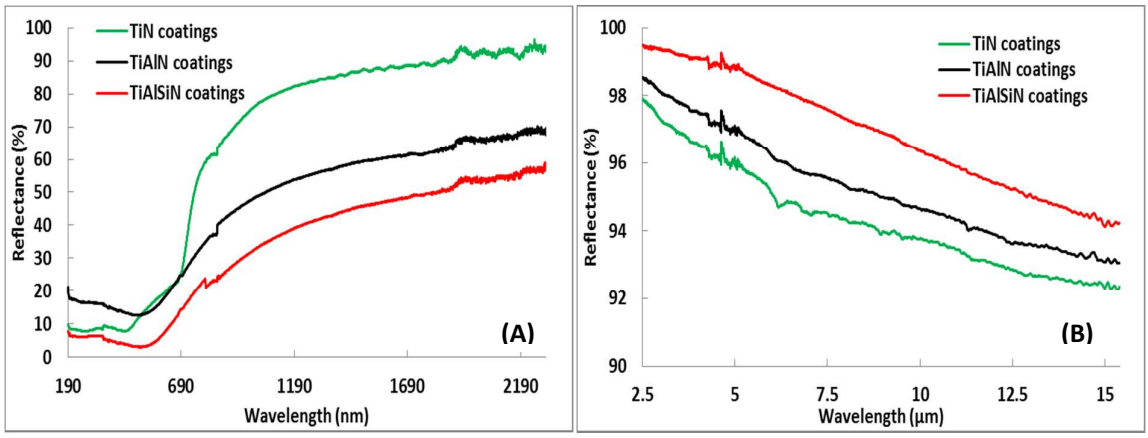

Figure 9. (A) UV-Vis and (B) FTIR reflectance spectra of the sputtered $Ti_xM_{1-x-y}N_y$ films (TiN, TiAlN and TiAlSiN respectively stand for $Ti_{0.5}N_{0.5}$, $Ti_{0.25}Al_{0.25}N_{0.5}$ and $Ti_{0.25}Al_{0.2}Si_{0.05}N_{0.5}$). Reprinted with permission from Ref. [62].

In order to harvest solar energy *via* solar thermal panels, researchers are persistently investigating for the developments of new materials to attain higher efficiencies by focusing on the constituent elements and structure features of the absorbing materials. Generally, a large number of materials have intrinsic absorption which is very low. For this reason, development of efficient solar selective materials by choosing appropriate materials and proper method is always in being in the hot spot. Typically, two phenomena can be successfully adopted to enhance the solar selective absorption: firstly, utilizing the interference effect of thin film coatings and optical trap to rise the solar absorptance and secondly, using an antireflective coating (ARC) on the top of the film surface to reduce thermal emittance and thereby increasing the absorptance [108-111]. In principle, the solar absorptance (in the visible range) and thermal emittance (in the infrared range) of a material depends on black coated layer, undercoating layer and substrates. The substrate and sublayer play very effective role to protect the solar selective absorbing layer against oxidation, diffusion, degradation, and corrosion at deleterious environmental conditions (mid to high temperature operations). Thus, a thermally stable diffusion barrier layer with superior optical properties can hinder diffusion of substrate into the solar selective absorbing surface.

Generally, solar selective surfaces are coated onto a highly reflective metal substrate [112] is due to the fact that on such developed spectrally selective surfaces the output temperature from solar collectors can be enhanced. In order to produce highly efficient, robust and low-

cost solar selective absorbers is adopting a highly reflective surface coated together with a highly absorbing spectrally selective surface which would work as absorber–reflector tandem assembly [113, 114]. As a result, lower emittance of the coating in the infrared region is due to the highly reflecting substrate and coated sublayer [115].

4. Other optical applications

Impressive structural diversity and good combinations of physical, mechanical, chemical, and electrical properties of transition metal nitrides make them useful to a wide range of applications across many practical fields. Generally nitride materials fall into two main classes: transition-metal nitrides and ionic-covalent nitrides [116]. In metal nitride thin film coatings, the metal-metal bonds are predominant whereas nitrogen-(non)metal bonds are preeminent in ionic covalent nitrides. According to the crystal symmetry and characteristic nature of transition-metal nitrides, they are very similar to carbides while the ionic-covalent nitrides are close to oxides. The optical properties of metal oxynitride and ionic-covalent oxynitride materials, and the influences of synthesis conditions and chemical structures on the optical properties of such materials are reviewed by Xie *et al*. [116]. The optical properties of these materials can be modified by controlling the compositions that alters the density of free electrons in their *d*-bands [20, 43]. The optical properties can be also regulated by integrating different metal elements into the metal nitride framework through converting bonding nature from metallic to covalent one [43]. For example, $Ti_{1-x}Al_xN$ coatings exhibit metallic characteristics with low Ti-content ($x \leq 0.48$) and dielectric behaviour with high Ti-content up to $x = 0.77$ [43]. Gradual improvement in the optical transmittance was noticed with the subsequent increase in aluminum content to the $Ti_{1-x}Al_xN$ coatings. Furthermore, coatings with $x < 0.5$ showed a maximum transmission and a maximum reflection in the visible region together with a high reflectance and low absorptance in the infrared region. The applications of transition metal nitride and carbide class materials in low temperature fuel cell technology have been investigated by various research groups as mentioned in previous review and researches [117, 118]. Extensive overviews on various optical parameters such as band-gap, refractive index, reflectance, absorptance, emittance, transmittance and photoluminescence of different oxynitride materials and their applications as selective solar surfaces, antireflection coatings, visible-light-driven photocatalysts, phosphors for light-emitting diodes, ecological pigments, and smart windows have been previously documented [17-20, 116]. The requirement of optical parameters of transition

metal nitride coatings vary from one application to another. In order to provide a better understanding, the property-structure (as well as associated efficiency for individual application) relationship the chemistry of different metal nitrides and their corresponding crystal structures have been overviewed by many groups [119-122].

Due to good thermal and chemical stability and hardness, metal nitride thin film coatings based have large number of technological applications as hard and superhard protective coatings, oxidation-, wear-, corrosion-, and erosion resistance coatings [1-3], microelectronic devices [123], ultraviolet and visible light emitters and detectors, and optical storage devices, optical devices such as active and passive optical planar waveguides, and antireflecting coatings [37-41], electronics devices, and diffusion barriers [43, 124]. Because of their large band-gap, high surface acoustic velocity, excellent chemical and thermal stability and physical robustness, these materials have secured their places in many optical devices as well. They are also popularly used in the semiconductor industry for optoelectronic devices at high power and high temperatures [125], in high temperature structural materials and gate dielectrics in microstructural devices [46, 126], and in spin-dependent photonic devices [11, 13, 127]. Introduction of suitable amount of dopants to the binary nitrides or oxynitrides results in band-gap engineering and design of emitters and detectors operating in the ultraviolet region. In an experimental investigation, metal-like CrN and wide-band gap semiconducting Cr_2O_3 was combined together by reactive dc magnetron sputtered system in $Ar/N_2/O_2(N_2O)$ atmospheres to deposit CrON and modify their band-gap and electronic properties for their optical and electronic applications [128]. Photothermal conversion of spectrally selective magnetron sputtered chromium oxynitride has been reported in a previous article [77]. Microstructural, electronic and optical characteristics of various chromium nitride coatings deposited by unbalanced reactive magnetron sputtering was performed by Logothetidis *et al*. [129]. The influence of nitrogen flow to the phase formation in Cr, Cr_2N, CrN coatings was investigated *via* XRD studies. Using Drude-Lorentz model [130, 131] together with the electronic structure of Cr_2N, CrN, the experimental results reckoned the metallic character of Cr_2N phase and the semiconducting nature of CrN structure [132, 133]. Nanocrystalline titanium nitride thin films found applications in different areas of semiconductor technology such as gate electrodes in field-effect transistors, Al diffusion barriers, and ultra-large scale integrated circuits [27-29]. Mutual interactions with the electrons in Ti and N atoms and the electronic structure of the stoichiometric titanium nitride affect the optical, electronic, and electrical behaviours of these nanocomposite films [130].

The complex dielectric function of TiN films was analysed on the basis of intra-band absorption and inter-band transitions in terms of the free electron Drude model and the Lorentz oscillator model respectively [130]. Furthermore, the combined Drude–Lorentz model was utilized to demonstrate the metallic nature of titanium nitride coatings and the origin of band structure modifications. In addition, the XRD and electron microscopy validated the spectroscopic ellipsometry results along with the insights on the atomistic mechanisms affecting the grains morphology and their correlation with the electronic and optical properties.

5. Summary and conclusions

We have reviewed the recent development of metal nitride and metal oxynitride thin film coatings, which are very prominent technological materials due to their outstanding physical properties and protective character, and for their optical and solar selectivity applications. Metal nitride based coatings *e.g.*, CrN, TiN, TiAlN, CrSiN, CrAlN, and NbN, have extensive industrial applications in cutting tools, in dry cutting, bearing spindles, metal forming, stamping dies, other mechanical machineries as well as automotive and aerospace applications because of their good wear resistance, thermal and corrosion resistance, good adhesion, high-temperature oxidation resistance, and a high level of hardness. These materials are also broadly used as optical, protective, and decorative coatings. Due to the combination of a large number of unique properties such as extraordinary thermal stability and superior optical properties, metal nitride based thin film coatings are considered to be one of the smartest aspirants in solar selective surface applications. Despite their technological importance, so far, there have been a very limited number of investigations on the solar selectivity features in the presence of various dopants. Optical responses of metal nitride based thin film coatings greatly vary from one application to another. As is mentioned previously, for the solar selective surface applications, these coatings must possess high solar absorptance to the visible light and low thermal emittance in the infrared region of the solar spectra. Until now, numerous binary, ternary and quarternary coatings *e.g.*, CrN, AlN, MoN, CrAlN, TiAlN, TiSiN, CrSiN, CrCN, CrMoN, CrON, CrWN, TiAlSiN, TiAlCrN, CrAlSiN, and CrMoSiN, have been extensively investigated. Among them TiAlN, TiAlSiN, CrON, ZrC-ZrN, NbAlN coatings have drawn more attention for their superior solar selectivity values (see Table 1) and thermal stability. Nevertheless, thorough research is still needed to further increase their mechanical properties, thermal and chemical stability and the oxidation

resistance behaviours of these materials before their place in the commercial market for industrial productions is confirmed.

Acknowledgements

Khalil Ibrahim and Hatem Taha gratefully acknowledge the financial support of Iraqi Government to carry out this research work. M Mahbubur Rahman gratefully acknowledges the support of Jahangirnagar University.

References

[1] A. Mycielski, L. Kowalczyk, R.R. Gałazka, R. Sobolewski, D. Wang, A. Burger, M. Sowińska, M. Groza, P. Siffert, A. Szadkowski, B. Witkowska, W. Kaliszek, Journal of Alloys and Compounds, 423 (2006) 163-168.

[2] F. Pan, C. Song, X.J. Liu, Y.C. Yang, F. Zeng, Materials Science and Engineering R: Reports, 62 (2008) 1-35.

[3] Y.C. Yang, F. Pan, Q. Liu, M. Liu, F. Zeng, Nano Letters, 9 (2009) 1636-1643.

[4] H. Morkoç, S. Strite, G.B. Gao, M.E. Lin, B. Sverdlov, M. Burns, Journal of Applied Physics, 76 (1994) 1363-1398.

[5] J.H. Edgar, Properties of Group III Nitrides, The Institution of Electrical Engineers, London, Wiley Online Library, UK (1994).

[6] X. Orignac, D. Barbier, X.M. Du, R.M. Almeida, Applied Physics Letters, 69 (1996) 895-897.

[7] R.M. Almeida, X. Orignac, D. Barbier, J Sol-Gel Sci Technol, 2 (1994) 465-467.

[8] K. Otsuka, C.V. Wayman, Shape Memory Materials, Cambridge University Press, Cambridge, UK, 1998.

[9] K. Otsuka, X. Ren, Progress in Materials Science, 50 (2005) 511-678.

[10] F. Zeng, C. Chen, B. Fan, Y.C. Yang, P.Y. Yang, J.T. Luo, F. Pan, W.S. Yan, Journal of Alloys and Compounds, 509 (2011) 440-446.

[11] M. Hashimoto, Y.K. Zhou, M. Kanamura, H. Asahi, Solid State Communications, 122 (2002) 37-39.

[12] M.S. Kim, Y.K. Zhou, M. Funakoshi, S. Emura, S. Hasegawa, H. Asahi, Applied Physics Letters, 89 (2006) 231511-232513.

[13] M.L. Reed, N.A. El-Masry, H.H. Stadelmaier, M.K. Ritums, M.J. Reed, C.A. Parker, J.C. Roberts, S.M. Bedair, Applied Physics Letters, 79 (2001) 3473-3475.

[14] J.L. Endrino, S. Palacín, A. Gutiérrez, F. Schäffers, J.E. Krzanowski, Journal of Materials Science, 42 (2007) 7607-7610.

[15] B.D. Beake, V.M. Vishnyakov, R. Valizadeh, J.S. Colligon, Journal of Physics D: Applied Physics, 39 (2006) 1392.

[16] P. Zeman, J. Musil, Applied Surface Science, 252 (2006) 8319-8325.

[17] K.E. Andersson, M. Veszelei, A. Roos, Solar Energy Materials and Solar Cells, 32 (1994) 199-212.

[18] C.G. Granqvist, Solar Energy Materials and Solar Cells, 91 (2007) 1529-1598.

[19] N. Selvakumar, H.C. Barshilia, Solar Energy Materials and Solar Cells, 98 (2012) 1-23.

[20] G.B. Smith, P.D. Swift, A. Bendavid, Applied Physics Letters, 75 (1999) 630-632.

[21] C. Mitterer, P.H. Mayrhofer, W. Waldhauser, E. Kelesoglu, P. Losbichler, Surface and Coatings Technology, 108-109 (1998) 230-235.

[22] P.E. Schmid, M.S. Sunaga, F. Lévy, Journal of Vacuum Science and Technology A: Vacuum, Surfaces and Films, 16 (1998) 2870-2875.

[23] P. Hones, R. Sanjines, F. Lévy, Surface and Coatings Technology, 94-95 (1997) 398-402.

[24] U. Beck, G. Reiners, I. Urban, K. Witt, Thin Solid Films, 220 (1992) 234-240.

[25] G. Reiners, H. Hantsche, H.A. Jehn, U. Kopacz, A. Rack, Surface and Coatings Technology, 54-55 (1992) 273-278.

[26] P. Zeman, R. Čerstvý, P.H. Mayrhofer, C. Mitterer, J. Musil, Materials Science and Engineering A, 289 (2000) 189-197.

[27] C.A. Dimitriadis, J.I. Lee, P. Patsalas, S. Logothetidis, D.H. Tassis, J. Brini, G. Kamarinos, Journal of Applied Physics, 85 (1999) 4238-4242.

[28] P. Patsalas, C. Charitidis, S. Logothetidis, C.A. Dimitriadis, O. Valassiades, Journal of Applied Physics, 86 (1999) 5296-5298.

[29] A. Satta, G. Beyer, K. Maex, K. Elers, S. Haukka, A. Vantomme, Materials Research Society Symposium - Proceedings, 612 (2000) D651-D656.

[30] G.G. Fuentes, E. Elizalde, J.M. Sanz, Journal of Applied Physics, 90 (2001) 2737-2743.

[31] S.V. Didziulis, J.R. Lince, T.B. Stewart, E.A. Eklund, Inorganic Chemistry, 33 (1994) 1979-1991.

[32] G.G. Fuentes, I.G. Mancheño, F. Balbás, C. Quirós, J.F. Trigo, F. Yubero, E. Elizalde, J.M. Sanz, Physica Status Solidi (A) Applied Research, 175 (1999) 429-436.

[33] L. Soriano, M. Abbate, H. Pen, P. Prieto, J.M. Sanz, Solid State Communications, 102 (1997) 291-296.

[34] C.G.H. Walker, C.A. Anderson, A. McKinley, N.M.D. Brown, A.M. Joyce, Surface Science, 383 (1997) 248-260.

[35] J.P.A.M. Driessen, A.D. Kuypers, J. Schoonman, Journal of Vacuum Science and Technology A: Vacuum, Surfaces and Films, 18 (2000) 1971-1976.

[36] M. Eizenberg, K. Littau, S. Ghanayem, M. Liao, R. Mosely, A.K. Sinha, Surfaces and Films, 13 (1995) 590-595.

[37] D. Barbier, X. Orignac, X.M. Du, R.M. Almeida, X. Orignac, D. Barbier, X.M. Du, R.M. Almeida, Proc. of Topical Symp. VII on Advanced Materials in Optics, Electro-Optics and Communication Technologies, 69 (1995) 33-897.

[38] H. Schroeder, Physics of Thin Films, Academic, New York, USA (1969).

[39] X. Orignac, D. Barbier, X.M. Du, R.M. Almeida, Applied Physics Letters, 69 (1996) 895-897.

[40] R.M. Almeida, X. Orignac, D. Barbier, Journal of Sol-Gel Science and Technology, 2 (1994) 465-467.

[41] Y. Sorek, R. Reisfeld, I. Finkelstein, S. Ruschin, Applied Physics Letters, 63 (1993) 3256-3258.

[42] H.C. Barshilia, N. Selvakumar, K.S. Rajam, D.V.S. Rao, K. Muraleedharan, A. Biswas, Applied Physics Letters, 89 (2006) 191909.

[43] A. Schüler, V. Thommen, P. Reimann, P. Oelhafen, G. Francz, T. Zehnder, M. Düggelin, D. Mathys, R. Guggenheim, Journal of Vacuum Science & Technology A: Vacuum, Surfaces, and Films, 19 (2001) 922-929.

[44] N. Hatcher, O.Y. Kontsevoi, A.J. Freeman, Physical Review B, 79 (2009) 020202.

[45] J. Cai, D.S. Wang, S.J. Liu, S.Q. Duan, B.K. Ma, Physical Review B, 60 (1999) 15691-15698.

[46] G. Petzow, M. Herrmann, Silicon Nitride Ceramics, in: M. Jansen (Ed.) High Performance Non-Oxide Ceramics II, Springer Berlin Heidelberg, Berlin, Heidelberg, Germany (2002).

[47] P. Dev, Y. Xue, P. Zhang, Physical Review Letters, 100 (2008) 117204.

[48] M. Dressel, G. Grüner, Electrodynamics of Solids: Optical Properties of Electrons in Matter, Cambridge University Press, Cambridge, UK (2003).

[49] A. Millar, M.M. Rahman, Z.-T. Jiang, Journal of Advanced Physics, 3 (2014) 179-193.

[50] M.M. Rahman, Z.-T. Jiang, Z.-f. Zhou, Z. Xie, C.Y. Yin, H. Kabir, M.M. Haque, A. Amri, N. Mondinos, M. Altarawneh, Journal of Alloys and Compounds, 671 (2016) 254-266.

[51] A. Amri, Z.T. Jiang, T. Pryor, C.-Y. Yin, S. Djordjevic, Renewable and Sustainable Energy Reviews, 36 (2014) 316-328.

[52] F. Cao, K. McEnaney, G. Chen, Z. Ren, Energy & Environmental Science, 7 (2014) 1615-1627.

[53] Z.Y. Nuru, D.E. Motaung, K. Kaviyarasu, M. Maaza, Journal of Alloys and Compounds, 664 (2016) 161-168.

[54] S. Esposito, A. Antonaia, M.L. Addonizio, S. Aprea, Thin Solid Films, 517 (2009) 6000-6006.

[55] C.A. Arancibia-Bulnes, C.A. Estrada, J.C. Ruiz-Suárez, Journal of Physics D: Applied Physics, 33 (2000) 2489.

[56] D. Xinkang, W. Cong, W. Tianmin, Z. Long, C. Buliang, R. Ning, Thin Solid Films, 516 (2008) 3971-3977.

[57] D. Gong, H. Liu, G. Luo, P. Zhang, X. Cheng, B. Yang, Y. Wang, J. Min, W. Wang, S. Chen, Z. Cui, L. Kewei, H. Lifang, Sol Energ Mater Sol Cells, 136 (2015) 167-171.

[58] L. Zheng, F. Zhou, Z. Zhou, X. Song, G. Dong, M. Wang, X. Diao, Solar Energy, 115 (2015) 341-346.

[59] G.D. Tang, Z.F. Shang, X.Y. Zhang, J. Xu, Z.Z. Li, C.M. Zhen, W.H. Qi, L.L. Lang, Physica B: Condensed Matter, 463 (2015) 26-29.

[60] M.M. Rahman, H.A. Miran, Z.-T. Jiang, M. Altarawneh, L.S. Chuah, H.-L. Lee, A. Amri, N. Mondinos, B.Z. Dlugogorski, RSC Advances, 7 (2017) 16826-16835.

[61] H. Kabir, M.M. Rahman, T.S. Roy, A.H. Bhuiyan, International Journal of Mechanical & Mechatronics Engineering, 12 (2012) 30-34.

[62] M.M. Rahman, Z.-T. Jiang, P. Munroe, L.S. Chuah, Z.-f. Zhou, Z. Xie, C.Y. Yin, K. Ibrahim, A. Amri, H. Kabir, M.M. Haque, N. Mondinos, M. Altarawneh, B.Z. Dlugogorski, RSC Advances, 6 (2016) 36373-36383.

[63] S.H. Wemple, M. DiDomenico Jr, Physical Review B, 1 (1970) 193-202.

[64] M. Yıldırım, F. Özel, N. Tuğluoğlu, Ö.F. Yüksel, M. Kuş, Journal of Alloys and Compounds, 666 (2016) 144-152.

[65] F. Yakuphanoglu, A. Cukurovali, I. Yilmaz, Physica B: Condensed Matter, 353 (2004) 210-216.

[66] B. BarIş, H.G. Özdemir, N. Tuğluoğlu, S. Karadeniz, O.F. Yüksel, Z. Kişnişci, Journal of Materials Science: Materials in Electronics, 25 (2014) 3586-3593.

[67] A.A.M. Farag, M. Fadel, Opt Laser Technol, 45 (2013) 356-363.
[68] M.M. El-Nahass, A.M. Farid, A.A. Atta, Journal of Alloys and Compounds, 507 (2010) 112-119.
[69] M.Y. Han, W. Huang, C.H. Chew, L.M. Gan, X.J. Zhang, W. Ji, Journal of Physical Chemistry B, 102 (1998) 1884-1887.

[70] C.G. Ribbing, A. Roos, Transition metal nitride films for optical applications, in: R.L. Hall (Ed.), San diego, CA, USA (1997).
[71] H.C. Barshilia, N. Selvakumar, K.S. Rajam, A. Biswas, Solar Energy Materials and Solar Cells, 92 (2008) 1425-1433.
[72] H.C. Barshilia, N. Selvakumar, K.S. Rajam, A. Biswas, Solar Energy Materials and Solar Cells, 92 (2008) 495-504.
[73] M. Du, L. Hao, J. Mi, F. Lv, X. Liu, L. Jiang, S. Wang, Solar Energy Materials and Solar Cells, 95 (2011) 1193-1196.
[74] S.A. Kalogirou, Progress in Energy and Combustion Science, 30 (2004) 231-295.
[75] C.E. Kennedy, H. Price, Progress in development of high-temperature solarselective coating, Proceedings of ISEC 2005, 520 (2005).
[76] Y. Liu, C. Wang, Y. Xue, Solar Energy Materials and Solar Cells, 96 (2012) 131-136.
[77] C. Nunes, V. Teixeira, M.L. Prates, N.P. Barradas, A.D. Sequeira, Thin Solid Films, 442 (2003) 173-178.
[78] N. Selvakumar, N.T. Manikandanath, A. Biswas, H.C. Barshilia, Solar Energy Materials and Solar Cells, 102 (2012) 86-92.
[79] S. Yue, S. Yueyan, W. Fengchun, Solar Energy Materials and Solar Cells, 77 (2003) 393-403.
[80] H.C. Barshilia, N. Selvakumar, K.S. Rajam, D.V. Sridhara Rao, K. Muraleedharan, Thin Solid Films, 516 (2008) 6071-6078.
[81] V. Godinho, D. Philippon, T.C. Rojas, N.N. Novikova, V.A. Yakovlev, E.A. Vinogradov, A. Fernandez, Solar Energy, 84 (2010) 1397-1401.
[82] H.C. Barshilia, N. Selvakumar, K.S. Rajam, Journal of Vacuum Science & Technology A, 25 (2007) 383-390.
[83] J. Huang, C. Xiang, S. Li, X. Zhao, G. He, Applied Surface Science, 293 (2014) 259-264.
[84] M. Du, L. Hao, X. Liu, J. Mi, L. Jiang, S. Wang, Procedia Engineering, 27 (2012) 6-11.

[85] L. Hao, M. Du, X. Liu, S. Wang, L. Jiang, F. Lü, Z. Li, J. Mi, Science China Technological Sciences, 53 (2010) 1507-1512.

[86] L. Hao, S. Wang, L. Jiang, X. Liu, H. Li, Z. Li, Chinese Science Bulletin, 54 (2009) 1451-1454.

[87] X.-H. Gao, Z.-M. Guo, Q.-F. Geng, P.-J. Ma, A.-Q. Wang, G. Liu, Solar Energy Materials and Solar Cells, 163 (2017) 91-97.

[88] J.-p. Meng, X.-p. Liu, Z.-q. Fu, K. Zhang, Solar Energy, 146 (2017) 430-435.

[89] A.G. Wattoo, C. Xu, L. Yang, C. Ni, C. Yu, X. Nie, M. Yan, S. Mao, Z. Song, Solar Energy, 138 (2016) 1-9.

[90] J. Jyothi, S. Latha, P. Bera, H.S. Nagaraja, H.C. Barshilia, Solar Energy, 139 (2016) 58-67.

[91] Z. Ke, D. Miao, H. Lei, M. Jianping, W. Jining, L. Xiaopeng, D. Zhejun, M. Jie, Z. Bo, Surface and Coatings Technology, 323 (2017) 65-71.

[92] A. Dan, J. Jyothi, K. Chattopadhyay, H.C. Barshilia, B. Basu, Solar Energy Materials and Solar Cells, 157 (2016) 716-726.

[93] T.K. Tsai, Y.H. Li, J.S. Fang, Thin Solid Films, 615 (2016) 91-96.

[94] B. Usmani, A. Dixit, Solar Energy, 134 (2016) 353-365.

[95] N. Selvakumar, K. Prajith, A. Biswas, H.C. Barshilia, Solar Energy Materials and Solar Cells, 140 (2015) 328-334.

[96] C. Zou, L. Huang, J. Wang, S. Xue, Solar Energy Materials and Solar Cells, 137 (2015) 243-252.

[97] H.C. Barshilia, Solar Energy Materials and Solar Cells, 130 (2014) 322-330.

[98] C. Wang, J. Shi, Z. Geng, X. Ling, Solar Energy Materials and Solar Cells, 144 (2016) 14-22.

[99] L. Rebouta, P. Capela, M. Andritschky, A. Matilainen, P. Santilli, K. Pischow, E. Alves, Solar Energy Materials and Solar Cells, 105 (2012) 202-207.

[100] P. Song, Y. Wu, L. Wang, Y. Sun, Y. Ning, Y. Zhang, B. Dai, E. Tomasella, A. Bousquet, C. Wang, Solar Energy Materials and Solar Cells, 171 (2017) 253-257.

[101] J. Jyothi, A. Biswas, P. Sarkar, A. Soum-Glaude, H.S. Nagaraja, H.C. Barshilia, Applied Physics A, 123 (2017) 496.

[102] A. Soum-Glaude, A. Le Gal, M. Bichotte, C. Escape, L. Dubost, Solar Energy Materials and Solar Cells, 170 (2017) 254-262.

[103] B. Li, D. Qi, X. Wang, F. Wang, Y. Nie, R. Gong, Materials Letters, 201 (2017) 5-8.

[104] Y. Ning, W. Wang, L. Wang, Y. Sun, P. Song, H. Man, Y. Zhang, B. Dai, J. Zhang, C. Wang, Y. Zhang, S. Zhao, E. Tomasella, A. Bousquet, J. Cellier, Solar Energy Materials and Solar Cells, 167 (2017) 178-183.

[105] Y. Ning, W. Wang, Y. Sun, Y. Wu, H. Man, C. Wang, S. Zhao, E. Tomasella, A. Bousquet, Y. Zhang, Infrared Physics & Technology, 80 (2017) 65-70.

[106] J. Zhang, T.P. Chen, Y.C. Liu, Z. Liu, H.Y. Yang, Solar Energy, 142 (2017) 33-38.

[107] C. Prieto, E. Céspedes, D. Hernández-Pinilla, A. Rodríguez-Palomo, O. Sánchez, F. Jiménez-Villacorta, E. Salas-Colera, MRS Advances, (2017) 1-8.

[108] T.K. Boström, E. Wäckelgård, G. Westin, Solar Energy Materials and Solar Cells, 84 (2004) 183-191.

[109] K. Forberich, G. Dennler, M.C. Scharber, K. Hingerl, T. Fromherz, C.J. Brabec, Thin Solid Films, 516 (2008) 7167-7170.

[110] C. Wang, J. Shi, Z. Geng, X. Ling, Solar Energy Materials and Solar Cells, 144 (2016) 14-22.

[111] A.D. Wilson, Solar Energy Materials, 10 (1984) 9-24.

[112] Z.C. Orel, Solar Energy Materials and Solar Cells, 57 (1999) 291-301.

[113] Z.C. Orel, M.K. Gunde, A. Lenček, N. Benz, Solar Energy, 69 (2000) 131-135.

[114] T. Tesfamichael, A. Hoel, E. Wäkelgård, G.A. Niklasson, M.K. Gunde, Z.C. Orel, Solar Energy, 69 (2000) 35-43.

[115] Z. Crnjak Orel, N. Leskovšek, B. Orel, M.G. Hutchins, Solar Energy Materials and Solar Cells, 40 (1996) 197-204.

[116] R.-J. Xie, H.T. Hintzen, Journal of the American Ceramic Society, 96 (2013) 665-687.

[117] D.J. Ham, J.S. Lee, Energies, 2 (2009) 873-899.

[118] B. Avasarala, P. Haldar, International Journal of Hydrogen Energy, 36 (2011) 3965-3974.

[119] D.H. Gregory, Coordination Chemistry Reviews, 215 (2001) 301-345.

[120] E. Kroke, M. Schwarz, Coordination Chemistry Reviews, 248 (2004) 493-532.

[121] R. Marchand, F. Tessier, A. Le Sauze, N. Diot, International Journal of Inorganic Materials, 3 (2001) 1143-1146.

[122] M. Zeuner, S. Pagano, W. Schnick, Angewandte Chemie - International Edition, 50 (2011) 7754-7775.

[123] B.D. Beake, V.M. Vishnyakov, R. Valizadeh, J.S. Colligon, Journal of Physics D: Applied Physics, 39 (2006) 1392-1397.

[124] H.C. Kim, T.L. Alford, Thin Solid Films, 449 (2004) 6-11.

[125] B.J. Arnold, S. Krishnamurthy, B. Kennedy, D. Cockburn, D. McNally, J.G. Lunney, R. Gunning, M. Venkatesan, J. Alaria, J. Michael, D. Coey, C. McGuinnessy, J.H. Guo, e-Journal of Surface Science and Nanotechnology, 7 (2009) 497-502.

[126] V.I. Belyi, A. Vasil'evich, Silicon Nitride in Electronics, Materials Science Monographs, 34 (1988).

[127] M.S. Kim, Y.K. Zhou, M. Funakoshi, S. Emura, S. Hasegawa, H. Asahi, S. Kimura, S. Emura, K. Tokuda, Y.K. Zhou, S. Hasegawa, H. Asahi, Appl. Phys. Lett, 89 (2006) 232511-232048.

[128] R. Mientus, R. Grötschel, K. Ellmer, Surface and Coatings Technology, 200 (2005) 341-345.

[129] S. Logothetidis, P. Patsalas, K. Sarakinos, C. Charitidis, C. Metaxa, Surface and Coatings Technology, 180-181 (2004) 637-641.

[130] P. Patsalas, S. Logothetidis, Journal of Applied Physics, 90 (2001) 4725-4734.

[131] P. Patsalas, S. Logothetidis, Journal of Applied Physics, 93 (2003) 989-998.

[132] D. Gall, C.S. Shin, R.T. Haasch, I. Petrov, J.E. Greene, Journal of Applied Physics, 91 (2002) 5882-5886.

[133] J. Häglund, G. Grimvall, T. Jarlborg, A.F. Guillermet, Physical Review B, 43 (1991) 14400-14408.